Distributed Hybrid Model Predictive Secondary Control of DC Microgrids with Random Communication Disorders

Meysam Yaribeygi, Zeinab Karami, Qobad Shafiee, *Senior Member*, *IEEE*, and Hassan Bevrani, *Fellow*, *IEEE*

***Abstract*—A reliable and robust communication network is essential to exchange information between distributed generators (DGs) and accurately calculate their control actions in microgrids (MGs). However, the integration of the communication network and MGs poses challenges related to the flexibility, availability, and reliability of the system. Furthermore, random communication disorders such as time delays and packet loss can negatively impact the system performance. Therefore, it is essential to design a suitable secondary controller (SC) with a fast dynamic response to restore voltage and appropriate power-sharing, while ensuring that the effects of random communication disorders are eliminated. In this regard, an optimal distributed hybrid model predictive secondary control method is presented in this paper. Realistic simulations are carried out in a mixed simulation environment based on MATLAB and OMNET++, by considering IEEE 802.11 (WiFi) using the recently developed Internet networking (INET) framework. In the implemented application layer, the *recoveryUnit* is responsible for reducing the impact of random communication disorders. The effectiveness and performance of the proposed method in comparison with a conventional model predictive control are verified by simulation results.**

***Index Terms*—Microgrid, model predictive control, random communication disorder, secondary control.**

I. Introduction

POWER electronics based systems are becoming increasingly popular for modern power systems such as microgrids (MGs) due to the increasing development and integration of renewable energy sources (RESs) [1]. Power electronic converters (PECs) are usually installed as an essential component in the MGs to improve efficiency, reduce emissions, and manage the variability of RESs. These components guarantee the principal duties of the MG such as voltage and frequency regulation, accurate power-sharing, as well as power balancing [2].

Direct current (DC) MGs are one of the future development trends due to their high efficiency, better power quality, and lower conversion losses, as well as their DC output characteristics in RESs (e.g., photovoltaic (PV)), electric vehicles (EVs), and energy storage systems (ESSs). In addition, DC MGs are not required to control frequency, phase, reactive power, harmonics, or power quality, which are all considerable challenges for alternating current (AC) MGs [3].

However, in a DC MG, voltage regulation, appropriate power-sharing, and plug-and-play (PnP) capability become more important issues that must be properly addressed, because in this case, the interaction between distributed energy resources (DERs) can lead to instability and failure including voltage fluctuation and voltage collapse [4]. To cope with these challenges and provide optimal solutions, advanced control of PECs in DC MGs is an important requirement [5]-[7]. The primary control is the fundamental control layer that locally ensures the system stability [8]. However, the primary control cannot adjust the voltage or frequency to nominal values when an MG is perturbed to track changes in power demand. Furthermore, the droop-based primary control method suffers from inherent voltage regulation and inappropriate current sharing due to its dependence on droop gain [9]. Indeed, voltage deviations and inaccurate current sharing in droop control caused by distinct output impedance characteristics are generally inescapable. Therefore, secondary control is employed to overcome these drawbacks [10]. This method can be categorized into three structures: centralized, decentralized, and distributed based on data exchanged by the communication network among DGs and a central control unit or only among DGs [11].

There are some reasons for the failure of centralized control including: ① the problem in redesigning a controller due to change even in an RES, ② high computational load due to the high number of controlled units, and ③ lack of availability of separate management units. In [12], decentralized control is proposed as the best option for presenting required functionalities; however, this control method ignores interactions between subsystems, which results in poor system performance.

Manuscript received: June 16, 2023; revised: September 17, 2023; accepted: November 7, 2023. Date of CrossCheck: November 7, 2023. Date of online publication: December 12, 2023.

M. Yaribeygi was with the Department of Electrical Engineering, K. N. Toosi University of Technology, Tehran, Iran, and he is now with the Sportradar Company, Trondheim, Norway (e-mail: yaribeygi@email.kntu.ac.ir).

Z. Karami (corresponding author) is with the Department of Engineering Cybernetics (ITK), Norwegian University of Science and Technology (NTNU), Trondheim, Norway (e-mail: zeinab.k.h.abadi@ntnu.no).

Q. Shafiee and H. Bevrani are with the Smart/Micro Grids Research Center, Department of Electrical Engineering, University of Kurdistan, Sanandaj, Iran (e-mail: q.shafiee@uok.ac.ir; bevrani@uok.ac.ir).

DOI: 10.35833/MPCE.2023.000417

To address the aforementioned challenges, the distributed secondary control (DSC) method has received much attention; additionally, this method satisfies stability, reliability, and scalability [13]-[16]. DSC is a control method that enables the coordination of multiple power sources and loads in MGs. This control method can be implemented through a communication network that connects the distributed control agents to each other. However, communication networks can be affected by various random communication disorders such as packet loss, delay, and transmission error, which can significantly affect the performance of the control method.

Recently, several methods such as those applying consensus algorithms, event-triggered control, and predicted control methods have been provided to improve the performance of secondary control in the presence of random communication disorders. An event-triggered secondary restoration control method aims to restore power supply in islanded MG after disturbances or faults [17]-[20]. This method allows each component to make its own independent decisions, which enhances the flexibility and robustness of the MG. A distributed event-triggered hierarchical control method has been proposed in [21]. In this method, control actions are coordinated across multiple levels and layers of the MG, incorporating economic objectives and enabling effective power management. Despite the fact that event-triggered strategies facilitate decentralized decision-making and reduce control overhead, they may face challenges when scaling up to larger MGs. The innovative distributed hierarchical control method introduced in [22] provides a resilient and secure method to improve the economic performance and stability of hybrid AC/DC MGs. It enables real-time management of DERs, voltage and frequency control, proportional power allocation, and economic power distribution, while ensuring data security and reducing the communication workload. Moreover, event-triggered control methods must demonstrate that the system does not exhibit Zeno behavior [23]. To avoid Zeno behaviors and reduce communication impairments, an optimal consensus-based control method is proposed in [24]. Furthermore, distributed optimization-based control methods such as model predictive control (MPC) have emerged.

MPC is an optimal control method that aims to solve an optimization problem over a prediction horizon at each sampling step with a fast dynamic response that can account for nonlinearity, uncertainty, and constraints of state and input variables in the controller design [25].

Generally, slowness control methods are usually designed at the secondary control level to ignore communication delays and deal the dynamics of the primary control level. While the secondary control methods need to be improved in order to have a fast dynamic response and excellent convergence speed. Therefore, the MPC methods have recently been explicitly and widely proposed in DC MGs as a secondary control strategy to reduce the communication delay [26]-[30]. Moreover, there are several advantages for using this method including ① robustness to delay: it is more robust to communication delay than infinite-time consensus algorithms for MGs; ② explicit optimization: MPC considers communication delays as part of the optimization problem and adjusts control actions to minimize their impact on system performance; ③ adaptability: MPC can adapt to varying communication delays in real-time, and adjust its predictions and control actions based on the most up-to-date information; and ④ MPC is well-suited for optimizing system performance over finite time horizons, and can achieve superior performance compared to infinite-time consensus algorithms. Although previous DSC based on MPC methods can guarantee current sharing and DC bus voltage restoration against communication constraints and uncertainties, some important issues have not been considered in previous papers. First, the accurate model of the MG and the various switching modes of PECs are ignored, leaving only the average value of the output voltages at the nominal value. Second, in order to mitigate the effects of communication disorders, the time delay is assumed to be constant, whereas in practical applications, the time delay is not deterministic. Finally, these methods have not been matched with constant power loads (CPLs), which may cause the filter's output to oscillate due to negative impedance characteristics in these loads.

This paper presents an optimal distributed hybrid model predictive secondary control method of DC MGs, which is a proper technique to compensate for random communication disorders and overcome the above challenges due to the dynamic network state. Although MATLAB provides meticulous physical models and many powerful functions, this simulation environment is not suitable for scheduling algorithms in communication network carrying real-time traffic. Therefore, simulations are implemented in a mixed simulation environment based on MATLAB and OMNET++ to reduce the overall computational burden. This could provide an efficient communication system to simulate high-complexity contexts. Due to developing the proposed method in the INET framework, a variety of data link layer protocols can be supported. Furthermore, IEEE 802.11 (WiFi) is considered because of its widespread usage in DSC of the networked microgrid (NMG). Moreover, to reduce the impact of stochastic communication disorders, a *recoveryUnit* is implemented, in which the lost data are predicted using previously stored data. The contribution of this paper can be summarized as follows.

1) As opposed to the MPC methods in [29]-[31], the proposed method presents an augmented model by considering the unknown disturbances as additive white Gaussian noise (AWGN) to guarantee stability and sensitivity as well as produce accurate voltage and current under existing perturbations.

2) Unlike the previous secondary control methods, this paper provides a novel DG architecture for NMGs in OMNET++ environment by incorporating both codes generated by C++ from MATLAB and properties of data communication network from INET framework, which supports both a variety of data link layer protocols and high programmability.

3) The proposed method provides flexibility and robustness for the system performance under stochastic communication disorders such as random delay and packet loss.

The remainder of this paper is structured as follows. In Section II, the system configuration is introduced in detail. The implementation process of the proposed method is discussed in Section III. In Section IV, simulation results are provided to confirm the performance of the proposed meth-

od. Finally, Section V concludes this paper.

II. System Configuration

This section describes some basic mathematical knowledge used in this paper. Necessary and sufficient graphical conditions are provided for structural controllability based on the communication topology of a DC MG. The detailed hierarchical control of the NMG including the electrical schematic of an DC MG with M DGs and DC/DC boost converters as well as the communication layer is demonstrated in Fig. 1, where VC and CC represent voltage control and current control, respectively.

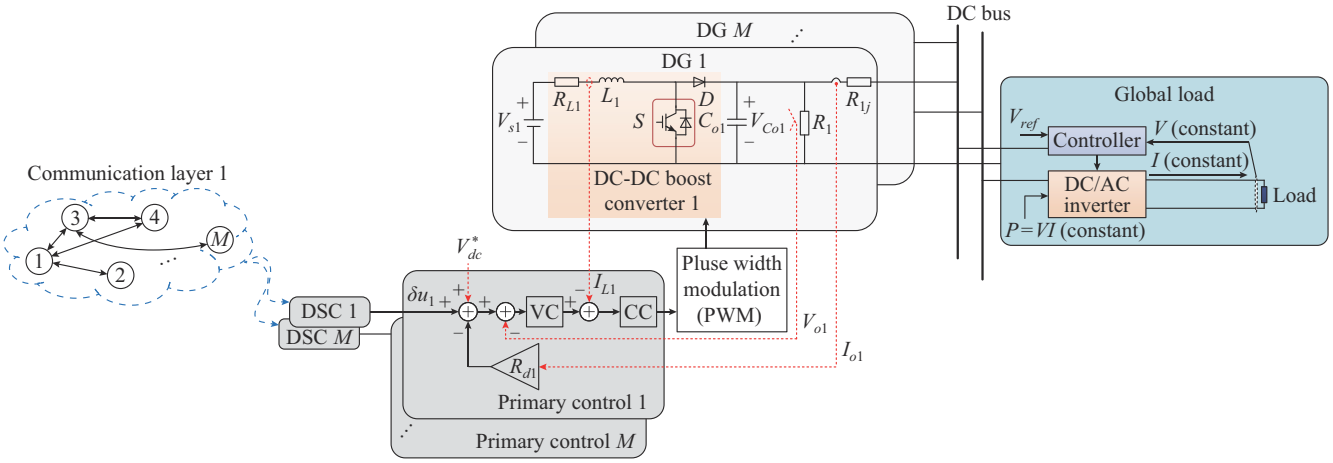

Fig. 1. Hierarchical control of NMG.

A. Data Communication Network Based on Graph Theory

The communication layer describes the information exchanged among the DGs (the i^{th} DG, $\forall i=1,2,...,M$), whose topology can be modelled by the graph theory $\boldsymbol{G}=(\boldsymbol{V},\boldsymbol{E},\boldsymbol{A})$, where $\boldsymbol{V}=\{\mathcal{V}_1,\mathcal{V}_2,...,\mathcal{V}_M\}$ is the set of nodes containing all DGs, $\boldsymbol{E}\subseteq\boldsymbol{V}\times\boldsymbol{V}$ is a set of the communication edge indicating the lines of the communication between DGs, and $\boldsymbol{A}=\{a_{ij}\}\in\mathbf{R}^{N\times N}$ is the adjacency matrix that represents the communication information and the communication weights. All the neighbors of node i are expressed as $\mathcal{N}_i=\{j|(\mathcal{V}_i,\mathcal{V}_j)\}$, where node j is called a neighbor of node i if there is a communication link from node i to node j. In other words, $\boldsymbol{E}=\{(\mathcal{V}_i,\mathcal{V}_j)|\text{if }\mathcal{V}_i\to\mathcal{V}_j\}$, where $\mathcal{V}_i\to\mathcal{V}_j$ means that if the information of the i^{th} DG can be transmitted to the j^{th} DG directly through communication network $\boldsymbol{G}$, then $a_{ij}>0$; else, $a_{ij}=0$. The Laplacian matrix of graph $\boldsymbol{G}$ is defined as $\boldsymbol{L}=\boldsymbol{D}_{in}-\boldsymbol{A}$, where $\boldsymbol{D}_{in}=\text{diag}\sum_{j=1}^{M}a_{ij}$ is a diagonal matrix (also known as the in-degree matrix). In addition, the out-degree matrix is denoted as $\boldsymbol{D}_{out}=\text{diag}\sum_{j=1}^{M}a_{ji}$. If in-degree and out-degree matrices are equal, the Laplace matrix $\boldsymbol{L}$ will be balanced. In this paper, for convenience, it is assumed that the graph of the communication network is strongly connected and weight-balanced to achieve an accurate current sharing and DC voltage regulation. It is easy to meet this assumption, as long as all DGs are connected, given that the communication channels between two DGs are bidirectional, i.e., $a_{ij}=a_{ji}$.

B. Physical Layer

The physical layer part from Fig. 1 illustrates a simplified electrical schematic model of i^{th} DG in a DC MG, where each DG is classified as a sub-system. The DC MG contains M DGs, each of which is composed of DC/DC boost converters so that the DG is represented by a constant voltage source with input voltage V_{si}. S and D are two power switches, where S is controllable, e. g., metal-oxide-semiconductor field-effect transistor (MOSFET) or insulate-gate bipolar transistor (IGBT), while D is uncontrollable. It is shown in the literature that the control performance of such system is more effective in the automatic model than in the averaged model [8]. Unlike the averaged model taking into account the switching modes, in the automatic model, the situation of inductor current in each sampling time is considered in addition to the switching modes. Therefore, in this paper, the automatic model is used, which is a completed model of the system. Details of the continuous-time model of the proposed system in averaged and automatic models with the switch positions are presented in [32]. The representation of the nonlinear state-space dynamic of the continuous-time equations of the automatic model can be calculated as follows:

$$\dot{\boldsymbol{x}}_i(t)=\begin{cases}\boldsymbol{A}_{1i}\boldsymbol{x}_i(t)+\boldsymbol{B}_i\boldsymbol{u}_i(t) & S=1, I_{Li}(t)>0\\ \boldsymbol{A}_{2i}\boldsymbol{x}_i(t)+\boldsymbol{B}_i\boldsymbol{u}_i(t) & S=0, I_{Li}(t)>0\\ \boldsymbol{A}_{3i}\boldsymbol{x}_i(t) & S=0, I_{Li}(t)=0\end{cases} \tag{1a}$$

$$\boldsymbol{y}_i(t)=\boldsymbol{C}_i\boldsymbol{x}_i(t) \tag{1b}$$

where $\boldsymbol{x}_i(t)=[I_{Li}(t),V_{Coi}(t)]^{\text{T}}$ is defined as the state variable vector including inductor current $I_{Li}(t)$ and capacitor voltage $V_{Coi}(t)$; $\boldsymbol{u}_i(t)=\boldsymbol{V}_{si}(t)$ is the input voltage; and $\boldsymbol{y}_i(t)$ is the output voltage of the i^{th} DG. Furthermore, assuming local and global loads in the form of a mix of resistance and constant power loads for each DG, matrices $\boldsymbol{A}_{1i}$, $\boldsymbol{A}_{2i}$, $\boldsymbol{A}_{3i}$, $\boldsymbol{B}_i$, and $\boldsymbol{C}_i$ are calculated as follows:

$$\boldsymbol{A}_{1i}=\begin{bmatrix}\dfrac{-R_{Li}}{L_i} & 0\\ 0 & \dfrac{-P}{C_{oi}V_{oi}^2}-\displaystyle\sum_{i=1}^{M}\sum_{j=1,j\neq i}^{M}\left(\frac{1}{R_{ij}}+\frac{1}{R_i}\right)\end{bmatrix} \tag{1c}$$

$$\boldsymbol{A}_{2i}=\begin{bmatrix}\dfrac{-R_{Li}}{L_i} & \dfrac{-1}{L_i}\\ \dfrac{1}{C_{oi}} & \dfrac{-P}{C_{oi}V_{oi}^2}-\sum_{i=1}^{M}\sum_{j=1,j\neq i}^{M}\left(\dfrac{1}{R_{ij}}+\dfrac{1}{R_i}\right)\end{bmatrix} \tag{1d}$$

$$\boldsymbol{A}_{3i}=\begin{bmatrix}0 & 0\\ 0 & \dfrac{-P}{C_{oi}V_{oi}^2}-\sum_{i=1}^{M}\sum_{j=1,j\neq i}^{M}\left(\dfrac{1}{R_{ij}}+\dfrac{1}{R_i}\right)\end{bmatrix} \tag{1e}$$

$$\boldsymbol{B}_i=\begin{bmatrix}\dfrac{1}{L_i} & 0\end{bmatrix}^{\mathrm{T}} \tag{1f}$$

$$\boldsymbol{C}_i=[0 \quad 1] \tag{1g}$$

where V_{oi} is the DC bus voltage of i^{th} DG; C_{oi} is the output capacitor filter; R_{Li} is the internal resistance of the input inductor L_i and C_{oi}; P is the power load on the DC bus side; and R_{ij} is the line impedance between the i^{th} DG and j^{th} DG or common bus; and the local loads of the i^{th} DG are considered as resistor R_i. It is assumed that the global load is the common CPL, i.e., $i_{CPL}=P/V_o$, where V_o is the DC bus voltage. Indeed, the nonlinear term associated with the CPL characteristics of the studied system can be defined by $-P/(C_{oi}V_{oi}^2)$, which appears in $A_{ji}(2,2)$.

C. Primary Control

The primary control, i.e., current control, voltage control, and droop control, is known as a local or internal control to regulate voltage and current with the preliminary power-sharing. This control level operates in the fastest response and preserves the voltage and power-sharing after sudden changes in demand or generation based on local measurements without communication links. However, conventional droop control is adopted to provide the current sharing between multiple DGs in a DC MG. With such mechanism, the performance depends on the amount of droop coefficients so that a large droop gains result in accurate current sharing but deviate the DC bus voltage severely from its nominal value and vice versa. Therefore, one of the drawbacks of droop control is the problem of DC bus voltage deviation, which is unable to be eliminated at this level. By properly tuning the proportional-integral (PI) control parameters of the inner loop and droop gain to achieve an adjustable current sharing ratio in the primary control layer, the output voltage of the i^{th} DG can be calculated as:

$$V_{oi,ref}=V_{dc}^{*}-R_{di}I_{oi} \tag{2}$$

where V_{dc}^{*} is the DC bus voltage reference; I_{oi} is the current of the i^{th} DG; and $R_{di}=\Delta V_{oi}/I_{oi,\max}$ is the droop gain, ΔV_{oi} is acceptable voltage change, and $I_{oi,\max}$ is the maximum rating current of the i^{th} DG.

D. Secondary Control

In order to achieve accurate system performance, a trade-off between power-sharing and voltage regulation performance is essential. In this regard, a secondary control level is provided, which is an effective solution to improve power allocation accuracy between DGs in a DC MG and restore the DC bus voltage at the same time compared with the traditional droop control method.

The secondary control maintains the control parameter in an optimization range by adding the secondary signal control input to the primary control in (2) as follows:

$$V_{oi,ref}=V_{dc}^{*}-R_{di}I_{oi}+\delta u_i \tag{3}$$

where δu_i is the voltage restoration term generated by the proposed DSC of the i^{th} DG.

III. Implementation Process of Proposed Method

This section presents an secondary control based on the hybrid model predictive control (HMPC) method as a distributed framework using an iterative algorithm, which allows for information to be exchanged during the sampling time. A voltage controller and a current controller are commonly used in the secondary control layer of the DC MGs. The steady-state deviations are a major problem regarding the performance indicators.

In contrast to the conventional droop mechanism, the proposed method can modify the operation point of the PC and eliminate steady-state deviations while providing voltage regulation and accurate current sharing. Since MPC is based on future predictions, this method uses the predicted values as known characteristics of the behavior of dynamic processes to achieve optimal conditions. While in the proportional-integral-derivative (PID) controller, the control actions are based on the past. When the secondary control is implemented and designed by the MPC method, the information transmitted typically consists of the future predicted values, so that any DSC can predict the interaction effects over the considered prediction horizon. The proposed DMPSC method is described in detail in the three stages listed below.

A. Stage 1: Measurement/estimation of Individual Parameters

The first stage to execute the proposed method is to obtain the required parameter information. In this regard, the output voltage V_{oi}, inductor current I_{Li}, input voltage V_{si}, and power load P of each DG, i.e., the i^{th} DG, are measured/estimated by the power link [33]. In addition, the predicted voltage and current deviations δV_{oj}^{n} and δI_{Lj}^{n} of other DGs are provided by the communication network, which are calculated in Stage 3.

B. Stage 2: Design of Proposed Method

This stage calculates the MPC commands. First, using measured/estimated values, the future behaviors of the DC MG (inductor current and output voltage of each DG in the current sample k) are predicted. Then, using these predicted values, as well as current and voltage references, a cost function is calculated to achieve the control objectives (i.e., current sharing and voltage regulation in DC MGs). Finally, the optimization problem in the MPC controller is determined by minimizing the cost function, as shown in Fig. 2.

1) Step 1: Discrete-time Model

The continuous state-space equation in (1) can be discretized using the Euler approximation as:

$$\frac{\mathrm{d}x(t)}{\mathrm{d}t}=\frac{x(k+1)-x(k)}{T_s} \tag{4}$$

where $k=nT_s$ ($n\in\mathbf{Z}^{+}$) is sample instant; and T_s is the sampling time of the controller.

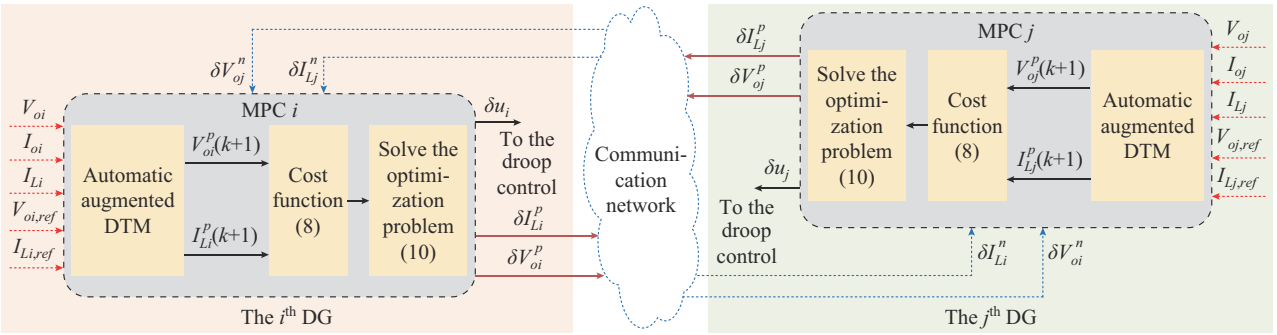

Fig. 2. Distributed implementation of DMPSC.

As previously stated, this paper considers an augmented automatic discrete-time model (DTM) of the system that takes into account all switching modes and inductor current situations given by (4) as an accurate model [8]. Furthermore, unknown disturbances are considered as AWGN, and the proposed solution can easily address the inherent fluctuations and uncertainties of the system.

$$\boldsymbol{X}_i(k+1)=\begin{cases}\bar{\boldsymbol{G}}_{1i}\boldsymbol{X}_i(k)+\bar{\boldsymbol{F}}_i\Delta\boldsymbol{v}_{si}(k)+\boldsymbol{W}_i(k)\\ \bar{\boldsymbol{G}}_{2i}\boldsymbol{X}_i(k)+\bar{\boldsymbol{F}}_i\Delta\boldsymbol{v}_{si}(k)+\boldsymbol{W}_i(k)\\ \bar{\boldsymbol{G}}_{3i}\boldsymbol{X}_i(k)+\boldsymbol{W}_i(k)\\ \bar{\boldsymbol{G}}_{4i}\boldsymbol{X}_i(k)+\dfrac{\tau_1}{T_s}\bar{\boldsymbol{F}}_i\Delta\boldsymbol{v}_{si}(k)+\boldsymbol{W}_i(k)\end{cases} \tag{5}$$

$$\boldsymbol{Y}_i(k)=\bar{\boldsymbol{H}}_i\boldsymbol{X}_i(k) \tag{6}$$

where $\boldsymbol{X}_i(k)=[\Delta\boldsymbol{x}_i(k),\boldsymbol{y}_i(k)]^{\mathrm{T}}$, $\bar{\boldsymbol{G}}_{mi}=\begin{bmatrix}\boldsymbol{G}_{mi} & \boldsymbol{O}^{\mathrm{T}}\\ \boldsymbol{H}_i\boldsymbol{G}_{mi} & \boldsymbol{I}_{q\times q}\end{bmatrix}$, $\Delta\boldsymbol{x}_i$, and $\Delta\boldsymbol{v}_{si}(k)$ are the differences between the states and the input vectors for the i^{th} DG, $m=1,2,3,4$ represents various equations based on different switching and inductor currents modes, $\boldsymbol{G}_{1i}=\boldsymbol{I}+T_s\boldsymbol{A}_{1i}$, $\boldsymbol{G}_{2i}=\boldsymbol{I}+T_s\boldsymbol{A}_{2i}$, $\boldsymbol{G}_{3i}=\boldsymbol{I}+T_s\boldsymbol{A}_{3i}$, $\boldsymbol{G}_{4i}=(\tau_1\boldsymbol{G}_{2i}+\tau_2\boldsymbol{G}_{3i})/T_s$, $\boldsymbol{H}_i=\boldsymbol{C}_i$, and $\boldsymbol{I}_{q\times q}$ is the identity matrix; i is the number of DGs available for installation, $i=1,2,...,M$; $\boldsymbol{W}_i(k)$ is the modeled disturbance and uncertainty as AWGN with $\sigma^2=0.1$; $\bar{\boldsymbol{F}}_i=\boldsymbol{B}_iT_s$; and $\tau_1+\tau_2=T_s$.

2) Step 2: Cost Function

The main objective of the proposed method is to ensure accurate current sharing between DGs so that the output voltage and the output current track the reference values with fast dynamic response and the minimum steady-state error. To accomplish this, the multi-objective cost function is defined below, which is made up of three weighted terms based on the control objectives. The first and second terms represent the average voltage restoration and the deviations between the individual current states and the reference value for N_p steps ahead, respectively, which are calculated as the local average of the predicted values of variables of the i^{th} DG, i. e., $V_{oi}^p(k+m)$ and $I_{Li}^p(k+m)$, and the information received from other DGs. The third term adjusts the overshoot and settling time. In other words, this term will penalize the sequence of control actions required to simultaneously carry out both the regulation and consensus objectives.

$$J_i(k)=\frac{1}{N_p}\left(\sum_{k=1}^{N_p}(\delta V_{oi}^p(k+1))^2+\sum_{k=1}^{N_p}(\delta I_{Li}^p(k+1))^2\right)+\gamma\sum_{k=0}^{N_u}(\delta V_{si}(k))^2 \tag{7}$$

where N_p and N_u are the prediction and control horizons, respectively; $V_{si}(k)$ is the control effort to obtain the best voltage reference to the primary control loop; and γ is the weighting coefficient penalizing relative big changes in $V_{si}(k)$, which defines a trade-off between the control effort and tracking and it can be calculated by the trial and error method. A weighting factor is used to balance control objectives and constraints that affect the performance of the proposed method. It is not easy to determine the appropriate weighting factors in order to achieve the desired behaviour of a system. In fact, to obtain the value of weighting factor, several factors such as the peak value, settling time, and oscillation magnitude must be taken into account. In this paper, the trial and error method is used to obtain the appropriate weighting factor. In this way, figures of merit are defined depending on the application, and a series of simulations are performed to find the most appropriate value [34]. Moreover, $\delta V_{oi}^p(k+1)$ and $\delta I_{Li}^p(k+1)$ for each DG are the local decision variables to achieve a minimum error tracking, which can be obtained as:

$$\begin{cases}\delta V_{oi}^p(k+1)=\dfrac{V_{oi}^p(k+1)+\sum_{i=1}^{M}\left(\sum_{j=1,j\neq i}^{M}\lambda_{ij}V_{oj}\right)}{1+\sum_{i=1}^{M}\left(\sum_{j=1,j\neq i}^{M}\lambda_{ij}\right)}-V_{o,ref}\\ \delta I_{Li}^p(k+1)=\dfrac{I_{Li}^p(k+1)+\sum_{i=1}^{M}\left(\sum_{j=1,j\neq i}^{M}\lambda_{ij}I_{Li}\right)}{1+\sum_{i=1}^{M}\left(\sum_{j=1,j\neq i}^{M}\lambda_{ij}\right)}-I_{Li,ref}\end{cases} \tag{8}$$

where V_{oi}^p, I_{Li}^p and V_{oj}, I_{Lj} are the prediction values of the state variables in the i^{th} DG and information communicated from the other DGs via communication network, respectively; $\lambda_{ij}=1$ if there is a communication link between the i^{th} and j^{th} DG, otherwise, it is zero; $V_{o,ref}$ is equal to V_{dc}^*; and $I_{Li,ref}$ at each sample instant k can be obtained as:

$$I_{Li,ref}(k)=\frac{I_{Li}^p(k)V_{oi}^p(k)}{V_{dc}^*} \tag{9}$$

3) Step 3: Optimization Problem

The proposed DSC has two outputs, which are the results of the local optimization problem. In this regard, the optimization problem for each DGs can be obtained by minimizing the given objective function as:

$$\begin{cases} \Delta U_i(k)=\arg\min J_i(k) \\ \text{s.t. } V_{oi,\min}\le V_{oi}^p(k+1)\le V_{oi,\max} \\ \quad I_{Li,\min}\le I_{Li}^p(k+1)\le I_{Li,\max} \\ \quad I_{Li}\ge 0 \\ \quad S=0 \text{ or } 1 \end{cases} \tag{10}$$

where $\Delta U_i(k)=\{\Delta X_i^p, \Delta u_i\}$ is the output of optimization problem with two subsets, which is provided as the proposed secondary controller. The first subset ΔX_i^p presents the set of predicted values of the state variables over the prediction horizon, and the second subset Δu_i represents the set of the control efforts provided below.

$$\begin{cases} \Delta X_i^p=\{\Delta V_{oi}^p(k), \Delta I_{Li}^p(k)\} \\ \Delta V_{oi}^p(k)=\{\delta V_{oi}^p(k), \delta V_{oi}^p(k+1), ...\} \quad k=0,1,...,N_p \\ \Delta I_{Li}^p(k)=\{\delta I_{Li}^p(k), \delta I_{Li}^p(k+1), ...\} \end{cases} \tag{11}$$

$$\Delta u_i=\{\delta u_i(k), \delta u_i(k+1), ...\} \quad k=0,1,...,N_u \tag{12}$$

According to the MPC principle, at each sampling time, only the first elements of each subset of the optimization problem results in (11) and (12) are applied. In this regard, the first element of the predicted control action i.e., $\delta u_i(k)$ is considered at $k-1$ instant, and is applied to the droop control as optimal secondary signal control to restore voltage deviation which can be obtained as (13). Moreover, the first elements of $\Delta V_{oi}^p(k)$ and $\Delta I_{Li}^p(k)$, which are a sequence of predicted voltage and current values, respectively, with switching sequences 2^{N_p}, are sent to the communication layer as the optimal predicted values. Finally, the calculated values δV_{oj}^n and δI_{Lj}^n in the communication layer are broadcasted via communication network to other DGs. The prediction horizon is shifted one step forward and these steps are then repeated each sample time with updated measurements/estimations.

$$\begin{cases} \delta u_i(k)=\delta V_i+\delta I_i \\ \delta V_i^n=\alpha_1\delta V_{oi}^p(k)+\alpha_2\sum_{j=1,j\ne i}^{M}\dfrac{\delta V_{oj}^p}{M-1} \\ \delta I_i^n=\beta_1\delta I_{oi}(k)+\beta_2\sum_{j=1,j\ne i}^{M}\dfrac{\delta I_{oj}^p}{M-1} \end{cases} \tag{13}$$

where δV_i is the voltage correction term; δI_i is used to provide an additional voltage correction term which can be used to compensate the line impedances to realize accurate current sharing; and α_1, α_2, β_1, and β_2 are the weighting coefficients reflecting the relative importance of the i^{th} controlled variables (inductive current and output voltage).

C. Stage 3: Communication Layer

This stage represents a mixed MATLAB/OMNET++ simulation environment to implement the proposed method. The OMNET++ simulator with MATLAB is presented as a common simulation model to reduce the overall computational load and provide an efficient communication system capable of simulating high-complexity fields. OMNET++ is an open-source, object-oriented, component-based discrete event simulator, which is gaining wide acceptance to develop simulations of communication networks, distributed hardware systems, multiprocessors, and protocol modeling.

In this paper, the proposed method is implemented using developed INET framework, which is an open-source model library for the OMNET++ simulation environment. The protocols, agents, and other models of communication networks have been provided by this framework. It includes internet stack models (transmission control protocol (TCP), user datagram protocol (UDP), open shortest path first (OSPE), IPv4, IPv6, etc.), types of link-layer protocols (Ethernet, PPP, IEEE 802.11, etc.), as well as many other protocols and components.

A snapshot from OMNET++ of the proposed method for the i^{th} DG (*distributedGeneration*) is shown in Appendix A Fig. A1. This model has been implemented by developing the application layer of the *standardHost* compound module of the INET framework. The developed application layer is composed of several simple modules. The *cppGeneratedCodes* simple module presents the physical and primary layers of DC MG, where the C++ source code for this simple module is generated from MATLAB. The proposed DSC method is implemented in *dMPSC*. This simple module runs in each sample time and its required inputs are received from *cppGeneretedCodes* and *recoveryUnit*, then its outputs are sent to the transport layer via *inetAPI*, which is an interface between the application layer and the transport layer that puts the inputs received from the *dMPSC* and the *currentTime* of the i^{th} DG in *voltage*, *current*, and *createdTime* fields of IP packets to be broadcasted to other DGs. When the packet has been received by *inetAPI* of the i^{th} DG, δV_{oi}^p and δI_{Li}^p are received, and τ_{ij} is extracted from (13); then they are sent to the *recoveryUnit*. τ_{ij} is the time delay of the communication network experienced by the IP packet that has been sent from the i^{th} DG to the j^{th} DG, which is calculated as:

$$\tau_{ij}=t_{cur,DG_j}-t_{cre,DG_i} \tag{14}$$

where t_{cur,DG_j} is the current time of the j^{th} DG; and t_{cre,DG_i} is the created time of the i^{th} DG.

The *recoveryUnit* is a unit for compensating the communication disorders that at each sample time must provide the required input values for the *dMPSC* module under any circumstances. The *recoveryUnit* consists of two tables to store the previous N values of voltage and current of other DGs. For example, a row of the voltage table of the i^{th} DG in *recoveryUnit* is shown in Fig. 3, where the voltage values of the j^{th} DG are stored.

δV_{oi}^p	$n-N$	…	$n-q$	…	$n-2$	$n-1$	n

Fig. 3. A row of voltage table of the i^{th} DG in *recoveryUnit*.

Whenever a packet is received, its voltage value is placed in position $n-q$ according to (15). On the other hand, at the n^{th} sampling time, if position n has a value, its value will be sent to the *dMPSC* module; otherwise, the value of position n will be predicted by regression and then sent to this module.

$$q=\begin{cases} 0 & \tau<D_{\min} \\ \left[\dfrac{\tau-D_{\min}}{N}\right]+1 & \tau>D_{\min} \end{cases} \tag{15}$$

where $D_{\min}$ is the minimum time delay which is considered based on communication instruction and network topology; and N is the size of the stored data, which depends on the

communication network quality so that in more unreliable networks, the larger value of N may be suitable.

Due to the focus on the fast response performance of the system in sudden changes, a nonlinear exponential function is used for regression as:

$$\bar{X}(x)=ae^{bx}+\xi \tag{16}$$

where ξ is independent normal with constant variance. The nonlinear regression can be moved to a linear domain by applying the log function:

$$\ln \bar{X}(x)=\ln a+bx \tag{17}$$

The goal is to find parameters a and b so that the mean-square error (MSE) is minimized, which is formulated as:

$$MSE=\frac{1}{N}\sum_{k=0}^{N}(\ln X(k)-\ln \bar{X}(k))^2 \tag{18}$$

To minimize the MSE, the reduced gradient is used which is derived in Algorithm 1, where α, β, and t are selected to be 0.01, 0.5, and 1, respectively; $\Delta \boldsymbol{x}$ is the learning rate and $\Delta \boldsymbol{x}=[0.0001, 0.0001]^{\mathrm{T}}$; and the initial values of model parameters are $\boldsymbol{x}=[0, 0]^{\mathrm{T}}$.

Due to the high importance of fast dynamic response in this paper, a user datagram protocol (UDP) is provided in the transport layer. The values of *voltage*, *current*, and *createdTime* are sent in 4-byte float format so the packet size of 64-byte is quite enough for UDP. IPv4 protocol is also used in the network layer and various protocols can be supported by the data link layer. Here, the IEEE 802.11 (WiFi) standard is selected for the data link layer, which is one of the most suitable options for the secondary control due to its low start-up cost, easy configuration and scalability, coverage distance (up to 100 m), and link rate (2 Mbit/s to 2.4 Gbit/s) [31]. Moreover, in the proposed method by selecting the IEEE 802.11 (WiFi) standard, the network will not enter into the heavy traffic. Traffic intensity is measured as $L\sigma/R$, where L is the packet size; σ is the input average rate that is proportional to switching frequency f_s; and R is the data link bandwidth.

Algorithm 1: reduced gradient

Require: $\alpha \in (0, 0.5)$, $\beta \in (0, 1)$, t, $\Delta \boldsymbol{x}=[\Delta \boldsymbol{x}_1, \Delta \boldsymbol{x}_2]^{\mathrm{T}}$ and $\boldsymbol{x}=[\boldsymbol{x}_1, \boldsymbol{x}_2]^{\mathrm{T}}$
Ensure: model parameters $\boldsymbol{x}$
Initialize parameters α, β, t, $\Delta \boldsymbol{x}$, and $\boldsymbol{x}$
Initialize convergence *innerTag* = *outerTag* = *False*
while *outerTag* = *False* **do**
  Compute $\boldsymbol{x}_1=\nabla_{x_1} f(\boldsymbol{x}_1, \boldsymbol{x}_2)$ and $\boldsymbol{x}_2=\nabla_{x_2} f(\boldsymbol{x}_1, \boldsymbol{x}_2)$
  while *innerTag* = *False* **do**
   if $f(\boldsymbol{x}_1+\Delta \boldsymbol{x}_1, \boldsymbol{x}_2+\Delta \boldsymbol{x}_2)>f(\boldsymbol{x}_1, \boldsymbol{x}_2)+\alpha t \nabla f(\boldsymbol{x}_1, \boldsymbol{x}_2)^{\mathrm{T}} \Delta \boldsymbol{x}$ **then**
    innerTag = *True*
   end if
  Update variable $t=\beta t$
  end while
  Update variable $\boldsymbol{x}=\boldsymbol{x}+t\Delta \boldsymbol{x}$
  if convergence condition holds **then**
   outerTag = *True*
  end if
end while
Return $\boldsymbol{x}$

IV. Simulation Results

In order to show the effectiveness of the proposed method, an islanded DC MG consisting of six DGs is considered. Each DG is driven by a DC/DC boost converter which supplies a common CPL, as shown in Fig. 4. The HMPC with the discrete augmented automatic model is simulated by using the fixed-step solver with sampling time $T_s=0.8$ ms. The MG model, control, and distribution network parameters can be obtained from Table I.

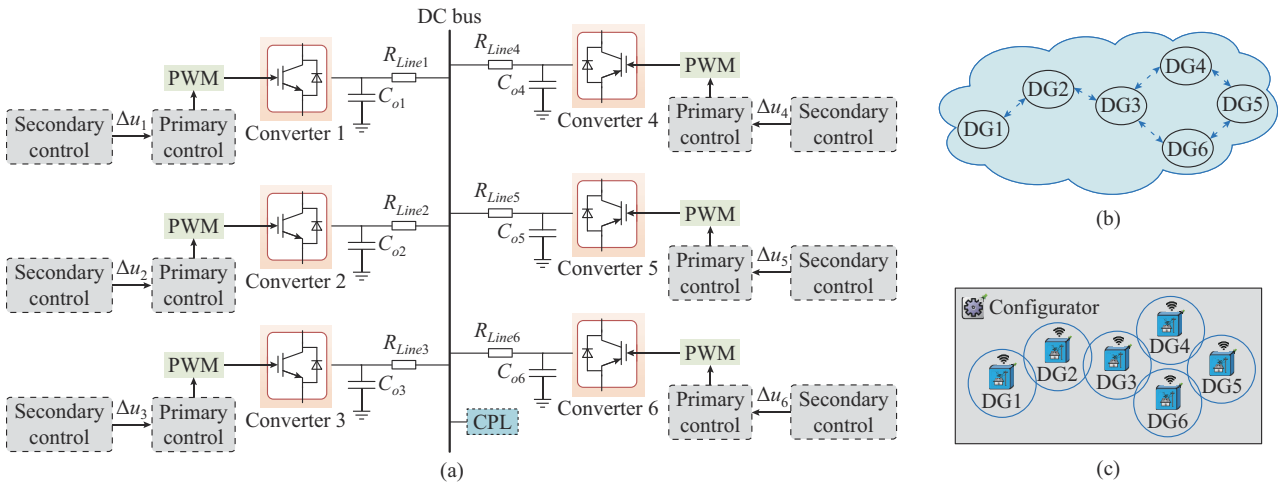

Fig. 4. Schematic of studied system. (a) DC microgrid with CPL. (b) Communication graph. (c) Snapshot from OMNET++.

Three different case studies have been provided to present the simulation results and verify the fast dynamic response of the proposed method. It is assumed that the first and second case studies have been investigated by considering an ideal communication topology, which means that the DC MG is considered without communication time delay between DGs, unlimited bandwidth, and zero bit-error rate. In addition, in the third case study, to confirm the effectiveness and robustness of the performance of the proposed method, four different non-idealist communication networks with a variety of random delay and packet loss are evaluated and compared with ideal communication. The size of the stored data N and $D_{\min}$ are selected to be 10 and 8 ms, respectively. Simulation results demonstrate the robustness and effectiveness of the proposed method with a fast dynamic response and without steady-state error.

TABLE I
ELECTRICAL AND CONTROL PARAMETERS

Parameter type	Parameter	Symbol	Value
Electrical parameters	Input voltage	V_{si}	150 V
	Voltage reference	V_{dc}^{*}	200 V
	Current reference of the i^{th} DG ($i=1,3,5$)	$I_{oi,ref}$	1 A
	Current reference of the i^{th} DG ($i=2,4,6$)	$I_{oi,ref}$	0.5 A
	Power load	P_{CPL}	900 W
	Inductor of the i^{th} converter	L_i	10 mH
	Capacitor of the i^{th} converter	C_{oi}	7 mF
	Resistance of the i^{th} converter	R_{Li}	0.1
	Line resistance	R_{Line1}, R_{Line3}, R_{Line5}	0.2
		R_{Line2}, R_{Line4}, R_{Line6}	0.4
Primary control parameters	Current control	K_{PIi}	0.5
		K_{IIi}	0.0002
	Voltage control	K_{PVi}	0.5
		K_{IVi}	10
	Droop gain of the i^{th} DG ($i=1,3,5$)	R_{di}	2
	Droop gain of the i^{th} DG ($i=2,4,6$)	R_{di}	4
Secondary control parameters	Sampling time	T_s	0.8 ms
	Weighting coefficient of the i^{th} DG ($i=1,2,...,6$)	α_1	1.8
		α_2	0.7
		β_2	0.2
	Weighting coefficient of the i^{th} DG ($i=1,3,5$)	β_1	0.4
	Weighting coefficient of the i^{th} DG ($i=2,4,6$)	β_1	0.8
	Prediction horizon	N_p	3
	Control horizon	N_u	2
	Weighting factor	γ	0.01

A. Comparison with Droop Control Under Load Change

In this case study, the current sharing test is conducted. In order to verify the proposed method, the system is considered with an ideal communication topology. The performance of the proposed method under load change has been demonstrated in Fig. 5. In Stage 1, when $t<2$ s, only the PC is activated and an additional CPL ($P_{CPL1}=300$ W) is attached to global load in common DC bus at $t=1$ s (power load increases from $P_{CPL}=900$ W to $P_{CPL}=1200$ W). In Stage 2, when $t\geq 2$ s, the proposed method begins to work. Voltage deviation is shown at $t=1$ s when the output power of CPL is suddenly changed. In this stage, due to the droop characteristic of the primary control, each voltage amplitude experiences a different deviation at most about 2.5 V, as shown in Fig. 5(c). At $t\geq 2$ s, the output voltage recovers to the rated value of 200 V for each DG unit at the same time under the proposed method, which can be successfully regulated and effectively restrain the voltage droop with fast response time and without only overshoot of the voltage, as shown in Fig. 5(a). After activating the proposed method, load change has been considered so that a CPL with $P_{CPL2}=230$ W is connected at $t=3.5$ s, then P_{CPL2} is disconnected from the grid at $t=4.5$ s. As can be observed, the proposed method recovers the current amplitude correctly after changing the load, and the voltage stability remains satisfactory.

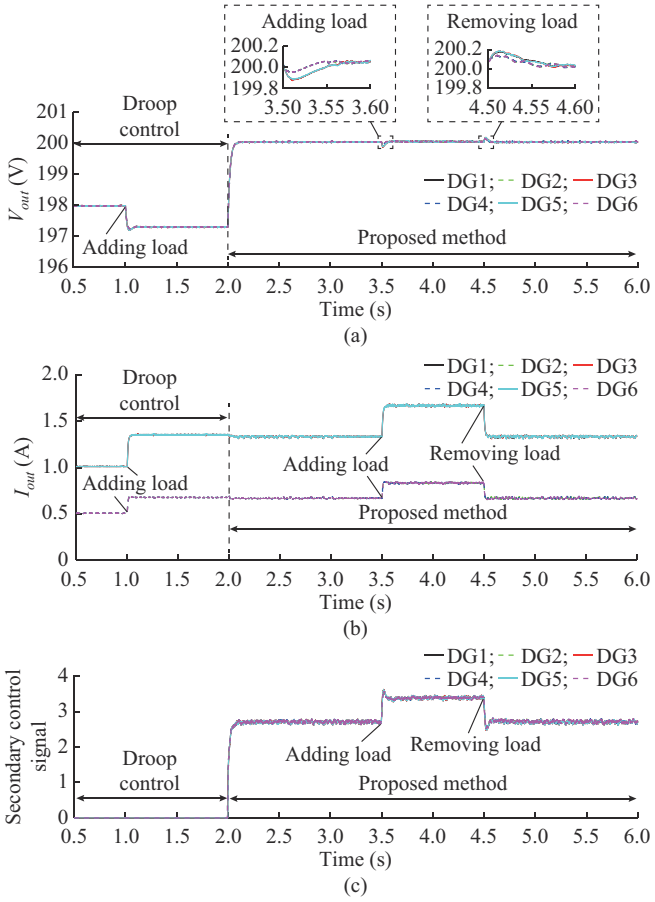

Fig. 5. Performance of proposed method under load change. (a) Output voltage. (b) Output current. (c) Secondary control signal.

In Fig. 5(b), current sharing has been illustrated in the DGs for each stage. It shows that current can be shared sufficiently between DGs according to the set ratios of the power of DGs, even before activating the proposed method by means of droop control, the currents recover stably when the CPL is changed at $t=1$ s, $t=3.5$ s, and $t=4.5$ s. Although the primary droop control is sufficient to share the current accurately, voltage regulation is provided inaccurately and is associated with a voltage deviation. As a result, the DC bus voltage stays at around 197.2 V instead of the nominal value (200 V). However, after activating the proposed method, it is able to supply the appropriate voltage quickly while maintaining the proper current sharing under frequent load changes.

B. Comparison Under PnP Capability and Communication Link Failure

The PnP scalability and capability as well as resiliency against communication link failure, which leads to the communication topology change, are studied in this case. Both primary droop control and the proposed method are in operation from the beginning, and the MG topology is shown in Fig. 6(a). It is assumed that DG3 is plugged off from the sys-

tem at $t=1.5$ s and plugged on at $t=2.5$ s, respectively. The DC MG topology is transformed as shown in Fig. 6(b).

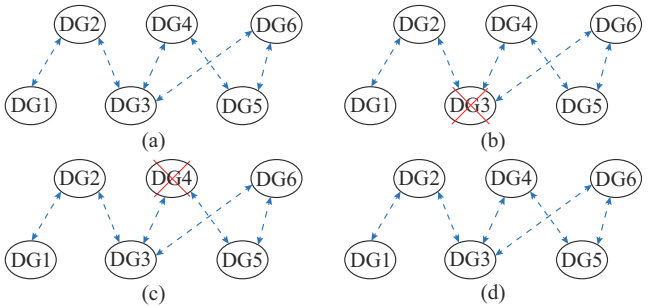

Fig. 6. Graph of communication topology. (a) $t<1.5$ s. (b) $1.5\ \text{s}<t<2.5$ s. (c) $4\ \text{s}<t<5$ s. (d) $t>5$ s.

Figure 7 illustrates the dynamic response of DGs due to this PnP operation.

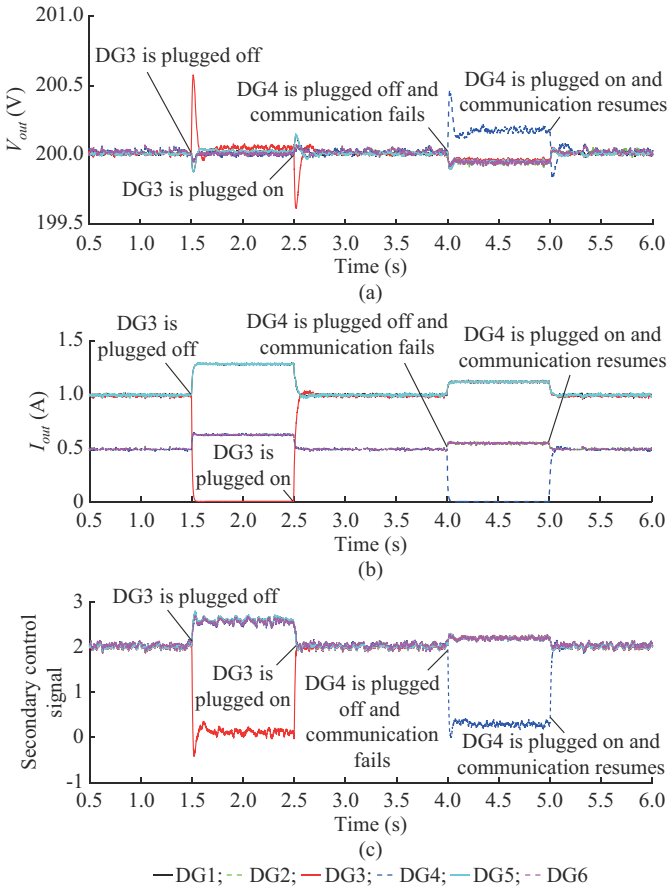

Fig. 7. Dynamic response of DGs due to PnP operation. (a) Output voltage. (b) Output current. (c) Secondary control signal.

As can be observed, when DG3 is disconnected and reconnected, the current can be shared quickly as desired among the DG units. Moreover, regardless of the connection and disconnection, the DC bus voltage can be well maintained at the nominal value. To further evaluate the effectiveness of the proposed method, the accuracy of the controller, and the robustness and capability against disconnection/connection of DGs and topology change, in the following text, it is assumed that DG4 is detached from the MG topology at $t=4$ s and is reconnected at $t=5$ s, so that all the communication links between DG4 and its neighbors are connected and disconnected at the same time. With the DG4 plugged off and the disconnection of communication links between DG4 and its neighbors, the MG topology becomes that in Fig. 6(c). Figure 7 demonstrates the dynamic responses, where the proposed method still drives the steady-state voltage regulation to the nominal values and keeps accurate current sharing with satisfied performance during and after the PnP operation and link failure. This illustrates that the proposed method is able to accommodate despite the uncertainties in the MG topology, causing only slight transients.

C. Comparison Under Random Delay and Packet Loss

In this case, a comparative simulation case is provided to verify the robustness of the proposed method under the effects of communication disorders. In this regard, the application layer of the *standardHost* compound module of the INET framework is developed.

Each packet experiences different latencies in each node that are randomly generated according to a Gaussian distribution $N(\mu,\sigma)$. This is exactly what happens in the real world for the packets. Although the time delays of communication technologies used in MGs have been reported to be less than 100 ms [35], in this paper, the average random time delay experienced by the packets in each node of low and high time delay networks is considered 12 ms and 25 ms, respectively, so the maximum time delays of these networks are 72 ms and 150 ms on average, respectively. Also, for the packet loss simulation, the packets are dropped by an average percentage. Despite it is reported that the packet losses for IEEE 802.11 in real world are varying between 5% and 45% [36], the selected packet losses are 20% and 50% for low and high packet loss networks, respectively.

Furthermore, in this case, the same stages are assumed as in case study 2. Figure 8 demonstrates the impact of random time delays and packet losses based on the proposed DSC by considering four different non-ideal communication networks compared with the ideal communication network. To confirm the performance of the proposed method, it is compared with conventional MPC under the same conditions. As observed in Fig. 8, the performance of the proposed method under low random time delay and packet loss is closer to the ideal communication network. While increasing time delay and packet loss makes it more difficult; however, the proposed method is able to reach the desired value with small fluctuation and steady-state error. In comparison with the conventional MPC, it is stated that the system performance reaches a new steady-state condition more slowly (about 0.4 s); in addition, it has large steady-state error and fluctuation in all case studies.

Moreover, it is observed that the system with conventional MPC is unstable under high time delay and packet loss with network types in Fig. 8(g) and 8(h). In contrast, the system using the proposed method under this case study can reach the steady state very quickly only after 0.05 s with a small fluctuation. Furthermore, the network types in Fig. 8(i) and 8(j) show the delay margin of the proposed method in which the system has been unstable under long time delay and packet loss.

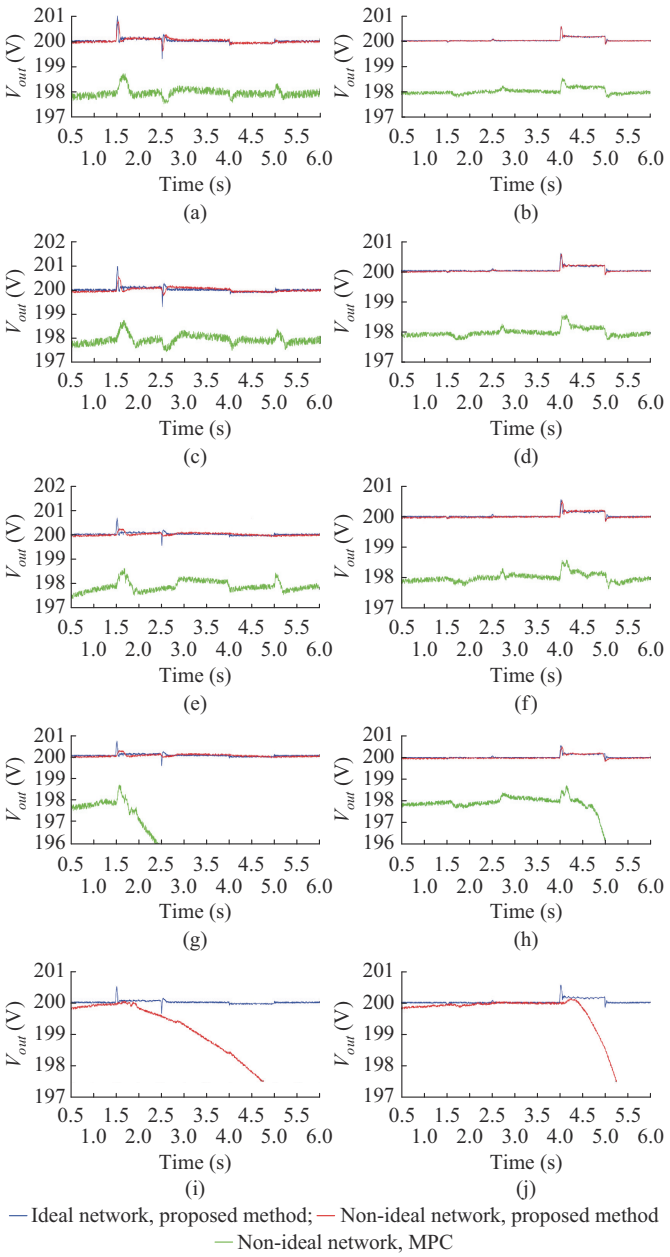

Fig. 8. Performance of proposed DSC in different communication networks under random time delay and packet loss. (a) Time delay follows $N(12, 2)$ ms, packet loss is 20%, DG3. (b) Time delay follows $N(12, 2)$ ms, packet loss is 20%, DG4. (c) Time delay follows $N(30, 6)$ ms, packet loss is 20%, DG3. (d) Time delay follows $N(30, 6)$ ms, packet loss is 20%, DG4. (e) Time delay follows $N(12, 2)$ ms, packet loss is 50%, DG3. (f) Time delay follows $N(12, 2)$ ms, packet loss is 50%, DG4. (g) Time delay follows $N(30, 6)$ ms, packet loss is 50%, DG3. (h) Time delay follows $N(30, 6)$ ms, packet loss is 50%, DG4. (i) Time delay follows $N(55, 10)$ ms, packet loss is 75%, DG3. (j) Time delay follows $N(55, 10)$ ms, packet loss is 75%, DG4.

V. Conclusion

In this paper, an optimal distributed hybrid model predictive secondary control method is presented to achieve fast voltage restoration and accurate power-sharing among DGs in islanded DC MGs. The proposed method has been evaluated to ensure desirable power-sharing, voltage regulation of DC buses, system scalability, and robustness to communication disorders. In this regard, the impact of random delay and packet loss has been assessed using a mixed simulation based on MATLAB and OMNET++. The studied DC MG is implemented by developing the application layer of the *standardHost* compound module of the INET framework. The *recoveryUnit* is implemented as a simple module in the application layer. In this unit, the predicted values of the HMPC are stored and the lost or delayed data are restored using the nonlinear regression method. The proposed method demonstrates how to extend the possibility of simultaneous stimulation of dynamic power system events and communication systems with the fast dynamic response using OMNET++ network simulator and C++ codes generated by MATLAB. The simulation results have confirmed the satisfactory performance of the proposed method.

Appendix A

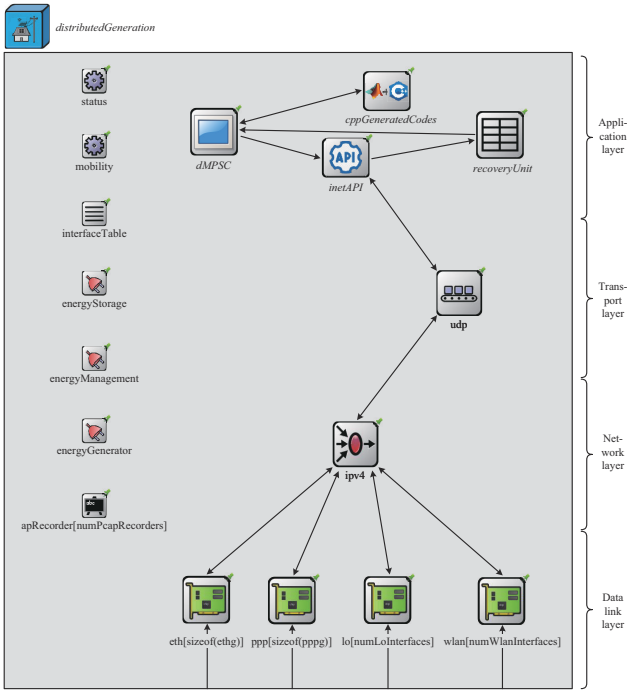

Fig. A1. Snapshot from OMNET++ of proposed method for the i^{th} DG.

References

[1] H. Bevrani, B. Francois, and T. Ise, *Microgrid Dynamics and Control.* Hoboken: John Wiley & Sons, 2017.

[2] Z. Karami, Q. Shafiee, and H. Bevrani, "Model predictive and sdre control of DC microgrids with constant power loads: a comparative study," in *Proceedings of 2018 Smart Grid Conference (SGC)*, Sanandaj, Iran, Nov. 2018, pp. 1-6.

[3] T. Dragicevic, X. Lu, J. C. Vasquez *et al.*, "DC microgrids – part I: a review of control strategies and stabilization techniques," *IEEE Transactions on Power Electronics*, vol. 31, no. 7, pp. 4876-4891, Sept. 2015.

[4] M. S. Sadabadi, Q. Shafiee, and A. Karimi, "Plug-and-play robust voltage control of DC microgrids," *IEEE Transactions on Smart Grid*, vol. 9, no. 6, pp. 6886-6896, Jul. 2017.

[5] F. Gao, R. Kang, J. Cao *et al.*, "Primary and secondary control in DC microgrids: a review," *Journal of Modern Power Systems and Clean Energy*, vol. 7, no. 2, pp. 227-242, Mar. 2019.

[6] S. Dahale, A. Das, N. M. Pindoriya *et al.*, "An overview of DC-DC converter topologies and controls in DC microgrid," in *Proceedings of 7th International Conference on Power Systems (ICPS)*, Pune, India, Dec. 2017, pp. 410-415.

[7] M. Srinivasan and A. Kwasinski, "Control analysis of parallel DC-DC converters in a DC microgrid with constant power loads," *Internation-*

al Journal of Electrical Power & Energy Systems, vol. 122, p. 106207, Nov. 2020.
[8] Z. Karami, Q. Shafiee, S. Sahoo *et al.*, "Hybrid model predictive control of DC-DC boost converters with constant power load," *IEEE Transactions on Energy Conversion*, vol. 36, no. 2, pp. 1347-1356, Dec. 2020.
[9] S. Peyghami, P. Davari, H. Mokhtari *et al.*, "Decentralized droop control in DC microgrids based on a frequency injection approach," *IEEE Transactions on Smart Grid*, vol. 10, no. 6, pp. 6782-6791, Apr. 2019.
[10] T. Khalili and A. Bidram, "Distributed control approaches for microgrids," in *Microgrids: Advances in Operation, Control, and Protection*. Cham: Springer, pp. 275-288, 2021.
[11] Y. Han, X. Ning, P. Yang *et al.*, "Review of power sharing, voltage restoration and stabilization techniques in hierarchical controlled DC microgrids," *IEEE Access*, vol. 7, pp. 149202-149223, Oct. 2019.
[12] C. Wang, J. Duan, B. Fan *et al.*, "Decentralized high performance control of DC microgrids," *IEEE Transactions on Smart Grid*, vol. 10, no. 3, pp. 3355-3363, Apr. 2018.
[13] X. Liu, Y. Wang, P. Lin *et al.*, "Distributed supervisory secondary control for a DC microgrid," *IEEE Transactions on Energy Conversion*, vol. 35, no. 4, pp. 1736-1746, May 2020.
[14] L. Xing, Y. Mishra, F. Guo *et al.*, "Distributed secondary control for current sharing and voltage restoration in DC microgrid," *IEEE Transactions on Smart Grid*, vol. 11, no. 3, pp. 2487-2497, Nov. 2019.
[15] J. Zhou, M. Shi, Y. Chen *et al.*, "A novel secondary optimal control for multiple battery energy storages in a DC microgrid," *IEEE Transactions on Smart Grid*, vol. 11, no. 5, pp. 3716-3725, Mar. 2020.
[16] L. Xing, Q. Xu, F. Guo *et al.*, "Distributed secondary control for DC microgrid with event-triggered signal transmissions," *IEEE Transactions on Sustainable Energy*, vol. 12, no. 3, pp. 1801-1810, Jul. 2021.
[17] M. Dong, L. Li, Y. Nie *et al.*, "Stability analysis of a novel distributed secondary control considering communication delay in DC microgrids," *IEEE Transactions on Smart Grid*, vol. 10, no. 6, pp. 6690-6700, Apr. 2019.
[18] L. Xing, Q. Xu, F. Guo *et al.*, "Distributed secondary control for DC microgrid with event-triggered signal transmissions," *IEEE Transactions on Sustainable Energy*, vol. 12, no. 3, pp. 1801-1810, Jul. 2021.
[19] J. Zhang, B. Sun, and D. Zhao, "A novel event-triggered secondary control strategy for distributed generalized droop control in microgrid considering time delay," *IEEE Transactions on Power Electronics*, vol. 38, no. 5, pp. 5963-5978, Jan. 2023.
[20] M. J. Najafirad, N. M. Dehkordi, M. Hamzeh *et al.*, "Distributed event-triggered control of DC microgrids with input saturation and time delay constraints," *IEEE Systems Journal*, vol. 17, no. 3, pp. 4786-4797, Sept. 2023.
[21] Z. Chen, X. Yu, W. Xu *et al*., "Modeling and control of islanded DC microgrid clusters with hierarchical event-triggered consensus algorithm," *IEEE Transactions on Circuits and Systems I: Regular Papers*, vol. 68, no. 1, pp. 376-386, Nov. 2020.
[22] Z. Li, Z. Cheng, J. Si *et al*., "Distributed event-triggered hierarchical control to improve economic operation of hybrid AC/DC microgrids," *IEEE Transactions on Power Systems*, vol. 37, no. 5, pp. 3653-3668, Dec. 2021.
[23] B. Abdolmaleki, Q. Shafiee, A. R. Seifi *et al*., "A zeno-free event-triggered secondary control for AC microgrids," *IEEE Transactions on Smart Grid*, vol. 11, no. 3, pp. 1905-1916, Oct. 2019.
[24] H. Wang, X. Ding, X. Wan *et al*., "Optimal-consensus-based event-triggered control strategy for island AC microgrids," *IEEE Systems Journal*, vol. 17, no. 3, pp. 3682-3693, Sept. 2023.
[25] A. Villalon, M. Rivera, Y. Salgueiro *et al*., "Predictive control for microgrid applications: a review study," *Energies*, vol. 13, no. 10, p. 2454, May 2020.
[26] N. Sheykhi, A. Salami, J. M. Guerrero *et al*., "A comprehensive review on telecommunication challenges of microgrids secondary control," *International Journal of Electrical Power & Energy Systems*, vol. 140, p. 108081, Sept. 2022.
[27] Z. Wang and C.-J. Ong, "Accelerated distributed MPC of linear discretetime systems with coupled constraints," *IEEE Transactions on Automatic Control*, vol. 63, no. 11, pp. 3838-3849, Feb. 2018.
[28] P. Liu and U. Ozguner, "Distributed model predictive control of spatially interconnected systems using switched cost functions," *IEEE Transactions on Automatic Control*, vol. 63, no. 7, pp. 2161-2167, Jul. 2018.
[29] Q. Yang, J. Zhou, X. Chen *et al*., "Distributed MPC-based secondary control for energy storage systems in a DC microgrid," *IEEE Transactions on Power Systems*, vol. 36, no. 6, pp. 5633-5644, May 2021.
[30] A. Navas-Fonseca, C. Burgos-Mellado, E. Espina *et al*., "Distributed predictive secondary control for voltage restoration and economic dispatch of generation for DC microgrids," in *Proceedings of IEEE Fourth International Conference on DC Microgrids (ICDCM)*, Arlington, USA, Jul. 2021, pp. 1-6.
[31] J. S. Gomez, D. Saez, J. W. Simpson-Porco *et al*., "Distributed predictive control for frequency and voltage regulation in microgrids," *IEEE Transactions on Smart Grid*, vol. 11, no. 2, pp. 1319-1329, Aug. 2019.
[32] Z. Karami, Q. Shafiee, Y. Khayat *et al*., "Decentralized model predictive control of DC microgrids with constant power load," *IEEE Journal of Emerging and Selected Topics in Power Electronics*, vol. 9, no. 1, pp. 451-460, Dec. 2019.
[33] R. Heydari, Y. Khayat, A. Amiri *et al*., "Robust high-rate secondary control of microgrids with mitigation of communication impairments," *IEEE Transactions on Power Electronics*, vol. 35, no. 11, pp. 12486-12496, Apr. 2020.
[34] P. Cortes, S. Kouro, B. La Rocca *et al*., "Guidelines for weighting factors design in model predictive control of power converters and drives," in *Proceedings of IEEE International Conference on Industrial Technology*, Seville, Spain, Mar. 2009, pp. 1-7.
[35] C. Kalalas, L. Thrybom, and J. Alonso-Zarate, "Cellular communications for smart grid neighborhood area networks: a survey," *IEEE Access*, vol. 4, pp. 1469-1493, Apr. 2016.
[36] A. P. Jardosh, K. N. Ramachandran, K. C. Almeroth *et al*., "Understanding link-layer behavior in highly congested IEEE 802.11b wireless networks," in *Proceedings of the 2005 ACM SIGCOMM Workshop on Experimental Approaches to Wireless Network Design and Analysis*, Philadelphia, USA, Aug. 2005, pp. 11-16.

Meysam Yaribeygi received the B.Sc. degree in electrical engineering from the University of Kurdistan, Sanandaj, Iran, in 2015, and the M.Sc. degree in electrical engineering-communication networks from the K. N. Toosi University of Technology, Tehran, Iran, in 2017. He is currently a Software Developer at Sportradar Company, Trondheim, Norway. His research interests include communication network, computer programming, microgrid, optimization, and software-defined networking.

Zeinab Karami received the B.Sc. and M.Sc. degrees from the University of Kurdistan, Sanandaj, Iran, in 2015 and 2017, respectively. She was a Researcher with the Smart/Micro Grids Research Center at the University of Kurdistan. She is currently pursuing the Ph.D. degree in the Department of Engineering Cybernetics (ITK), Norwegian University of Science and Technology (NTNU), Trondheim, Norway. Her main research interests include control of power electronic converters, microgrid stability, model predictive control, nonlinear, optimal, and robust control for the application of power electronics and wireless power transfer charging system.

Qobad Shafiee received the Ph.D. degree in electrical engineering from the Department of Energy Technology, Aalborg University, Aalborg, Denmark, in 2014. He is currently an Associate Professor and Co-leader of the Smart/Micro Grids Research Center at the University of Kurdistan, Sanandaj, Iran, where he was a Lecturer from 2007 to 2011. In 2014, he was a Visiting Scholar with the Electrical Engineering Department, the University of Texas at Arlington, Arlington, USA. He was a Post-doctoral Fellow and Visiting Professor with the Department of Energy Technology, Aalborg University, in 2015 and 2017, respectively. His current research interests include dynamic modelling, stability, security, and control of power electronics-based system and microgrid, and model predictive and optimal control of modern power system.

Hassan Bevrani received the Ph.D. degree in electrical engineering from Osaka University, Osaka, Japan. Currently, he is a Professor and the Program Leader of Smart/Micro Grids Research Center (SMGRC) at the University of Kurdistan, Sanandaj, Iran. Over the years, he has worked as a Senior Research Fellow and Visiting Professor at Osaka University, Kumamoto University (Japan), Kyushu Institute of Technology (Japan), Doshisha University (Japan), Nagoya University (Japan), Queensland University of Technology (Australia), Centrale Lille (France), and Technical University of Berlin (Germany). His current research interests include microgrid dynamics and control, smart grid operation and control, and intelligent/robust control application in power electric industry.